Integrated nanopore sensing platform with sub-microsecond temporal resolution

Jacob K Rosenstein[1], Meni Wanunu[2,3], Christopher A Merchant[3], Marija Drndic[3] & Kenneth L Shepard[1]

Nanopore sensors have attracted considerable interest for high-throughput sensing of individual nucleic acids and proteins without the need for chemical labels or complex optics. A prevailing problem in nanopore applications is that the transport kinetics of single biomolecules are often faster than the measurement time resolution. Methods to slow down biomolecular transport can be troublesome and are at odds with the natural goal of high-throughput sensing. Here we introduce a low-noise measurement platform that integrates a complementary metal-oxide semiconductor (CMOS) preamplifier with solid-state nanopores in thin silicon nitride membranes. With this platform we achieved a signal-to-noise ratio exceeding five at a bandwidth of 1 MHz, which to our knowledge is the highest bandwidth nanopore recording to date. We demonstrate transient signals as brief as 1 μs from short DNA molecules as well as current signatures during molecular passage events that shed light on submolecular DNA configurations in small nanopores.

Single-molecule measurements are attractive not only for their extremely high sensitivity but also for the insight that they offer into molecular features that are masked in ensemble measurements. Over the past several decades, a variety of fluorescence-based techniques have enabled both *in vivo* and *in vitro* studies of the structure, function and dynamics of single molecules[1]. However, optical single-molecule techniques generally cannot directly resolve temporal changes that occur on sub-millisecond timescales, as imaging times must accommodate the relatively slow rate of photon emission from a single fluorophore.

In contrast, non-optical techniques that offer direct transduction to ion or electron flux can enable studies of dynamic single-molecule processes on microsecond or nanosecond timescales. Nanopore sensors have emerged as one such tool with potential for observing single molecules at high throughput and with fine temporal resolution. A nanopore sensor comprises an insulating membrane with a single nanometer–scale aperture. When both sides of the membrane are exposed to electrolyte solutions, a solitary electrolyte junction forms at the nanopore. An electrode is placed in each solution, and an applied voltage results in a steady-state ionic flux through the pore. The presence of a single analyte molecule causes a transient change in the ionic conductance of the pore, which one observes as an electrical current pulse for each passing molecule. The shape and statistical properties of these pulses are useful for analyzing a biomolecular species in solution. Nanopores can be constructed by a variety of techniques, including biological pores formed by transmembrane proteins[2] and synthetic pores fabricated from various materials[3].

In addition to their use for biophysical studies, nanopores are a candidate for improved DNA sequencing platforms[4], potentially offering extremely high throughput and very long read lengths. However, the transient nature of nanopore signals presents a major limitation; typical velocities of nucleic acids passing through solid-state nanopores, for example, are 10–1,000 ns per base. Despite ongoing efforts to reduce translocation speeds, 'fast' translocations are often cited as a critical barrier to the progress of nanopore sensing applications[5]. Recent work using an enzyme molecule as a molecular ratchet[6] appears particularly promising in this respect. Although the signals from nanopores represent a flux of several billion ions per second, in practice nanopore measurements have been constrained to bandwidths below 100 kHz owing to comparatively high background noise.

In this work we consider the bandwidth limitations of conventional nanopore measurements and demonstrate a CMOS-integrated nanopore platform (CNP) that supports signal bandwidths exceeding 1 MHz by exploiting a custom micrometer-scale amplifier optimized for nanopore sensing, integrated in immediate proximity to the pore. We demonstrated the utility of this platform by detecting, to our knowledge for the first time, single-microsecond interactions of individual molecules with nanopores, which enabled us to observe multiple distinct configurations of a short DNA molecule during its passage through a solid-state nanopore.

RESULTS

Sensing platform

The CNP centers around a custom-designed, low-noise current preamplifier and a high-performance solid-state nanopore. The preamplifier circuitry occupies 0.2 mm^2 in a 0.13-μm mixed-signal

[1]Department of Electrical Engineering, Columbia University, New York, New York, USA. [2]Departments of Physics and Chemistry and Chemical Biology, Northeastern University, Boston, Massachusetts, USA. [3]Department of Physics, University of Pennsylvania, Philadelphia, Pennsylvania, USA. Correspondence should be addressed to K.L.S. (shepard@ee.columbia.edu) or J.K.R. (jrosenstein@ee.columbia.edu).

RECEIVED 11 NOVEMBER 2011; ACCEPTED 23 FEBRUARY 2012; PUBLISHED ONLINE 18 MARCH 2012; DOI:10.1038/NMETH.1932

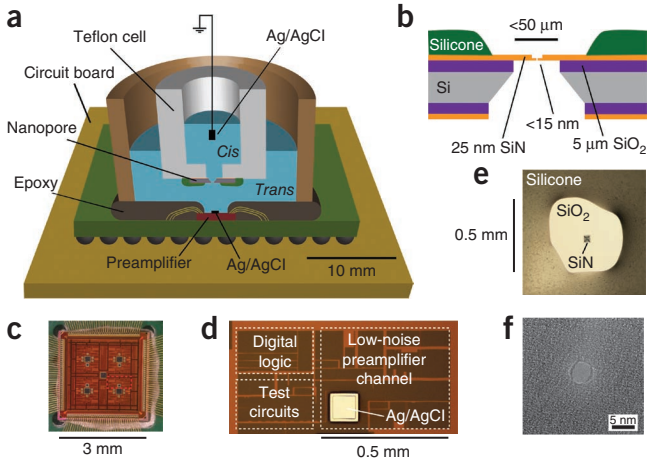

Figure 1 | The CNP. (**a**) Schematic of the measurement setup. (**b**) Cross-section schematic of the low-capacitance thin-membrane chip. (**c**) Optical micrograph of the 8-channel CMOS voltage-clamp current preamplifier. (**d**) Magnified image of one preamplifier channel. (**e**) Optical image of a solid-state silicon nitride membrane chip mounted in the fluid cell. (**f**) Transmission electron microscope image of a 4-nm-diameter silicon nitride nanopore.

CMOS process and is positioned directly inside the fluid chamber (**Fig. 1**). We placed a thin silicon nitride nanopore[7] in the chamber above the amplifier (Online Methods). This design considerably reduced parasitic capacitances, resulting in lower high-frequency noise than in traditional platforms that rely on external electrophysiology amplifiers such as the Axopatch 200B (Molecular Devices) or EPC-10 (HEKA Electronik). The CNP's planar amplifier design is also well-suited to parallelization, and with the addition of fluidics to isolate the *trans* chambers of an array of nanopores, the platform can support multichannel detection.

Bandwidth and noise in nanopore sensors

Analysis of bandwidth in nanopore sensing systems is similar to the analysis of voltage-clamp electrophysiology recordings[8,9], except that the magnitudes of contributing elements can vary considerably. Both of these systems produce weak ionic currents, and their useful signal bandwidths are generally constrained not by small-signal frequency response but by the signal-to-noise ratio (SNR). Detailed treatments of noise in ion-channel recordings[8] often address scenarios with signal amplitudes of 10 pA or less, for which relevant bandwidths are typically less than 10 kHz. However, nanopore sensors often use more concentrated electrolytes and higher holding potentials, producing current pulses of 100 pA from α-hemolysin[2], 300 pA for MspA[10] and upward of 4 nA for solid-state nanopores[7].

A nanopore can be modeled as an ionic resistance, R_P, in series with an access resistance, R_A[11], along with a capacitance from its supporting membrane, C_M (**Fig. 2a**). In addition, capacitance is associated with the measurement electronics (**Fig. 2b**,**c**), with contributions from the electrode wiring (C_W), the amplifier input (C_I) and the amplifier feedback elements (C_F). Current (I) signals from nanopores are usually transient and described by their depth (ΔI) and duration (τ) (**Fig. 2d**).

In the low-frequency regime (<100 Hz), nanopore noise power spectral density is dominated by flicker noise arising from fluctuations in the pore's ionic conductance[12]. At moderate frequencies (100–10,000 Hz), sources of white noise in the pore[13] or measurement electronics may appear, along with noise generated by energy dissipation in non-ideal dielectric materials (**Fig. 2e**). Finally, at frequencies >10 kHz, the dominant noise source is the interaction of the amplifier's voltage noise with the total capacitance at the input. In this regime, the input-referred power spectral density is

$$S_n(f) \approx (2\pi f(C_M + C_W + C_I + C_F)v_n)^2$$

and root-mean-squared current noise is

$$I_{RMS}(B) \approx (2\pi/\sqrt{3})B^{3/2}(C_M + C_W + C_I + C_F)v_n$$

where v_n is the voltage noise density (V/√Hz) of the input amplifier, and B is the measurement bandwidth.

To arrive at an SNR metric, previous studies[12,14] have defined the signal as ΔI, the average change in current caused by the presence of a molecule in the pore. The corresponding metric is then $SNR(B) = \Delta I / I_{RMS}(B)$. To more accurately evaluate performance for brief events, we instead redefined $SNR(B,\tau)$ as a function of both bandwidth and pulse duration (**Supplementary Discussion**). One consequence of this modification is that if a signal contains brief transient events, the SNR may increase for wider bandwidths despite greater I_{RMS} values.

From this analysis, we can define the maximum bandwidth (B_{max}) at which the SNR exceeds a minimum value (SNR_{min}). If $\tau < 100$ µs and $B > 1/(2\tau)$, this upper bound is given by

$$B_{max} \approx \left(\frac{\Delta I \sqrt{3}}{SNR_{min} \times 2\pi(C_M + C_W + C_I + C_F)v_n} \right)^{\frac{2}{3}}$$

The minimum tolerable SNR will vary, but to avoid substantial false event detection rates it can be reasonable to require an SNR of 5 or more (**Supplementary Discussion**). Regardless of the exact requirements, it is clear that the available bandwidth increases for larger signal levels (ΔI) and decreases for larger capacitances and amplifier voltage noise. All of the capacitances in this expression are extrinsic to the nanopore and, therefore, eligible for improvement without affecting the properties of the pore itself.

Reducing parasitic capacitances through integration

Nanopore signal fidelity is extremely sensitive to parasitic electronic elements at the amplifier input, including any capacitance from the pore membrane (**Fig. 2a**). Solid-state nanopores are fabricated in thin dielectric membranes, and C_M can be modeled by the parallel-plate capacitance of the constituent elements of the membrane (**Supplementary Discussion**). Early silicon nitride nanopores had C_M > 300 pF[12]. For the nanopores used here (**Fig. 1**), a thin SiN film was supported by a thick SiO_2 layer, and additionally the surface of the membrane chip was covered with a silicone elastomer, leaving only a minimal area exposed to the electrolyte (Online Methods). As a result, C_M was reduced to <6 pF. Additional fabrication efforts should allow C_M to be reduced below 0.5 pF[15].

The close integration of the measurement electronics also reduces C_W. In conventional platforms, C_W results from any capacitive coupling to other nodes (often >2 pF) from the short length (<10 cm) of wire that connects one electrode to the amplifier input. In the CNP design, a silver–silver chloride (Ag/AgCl)

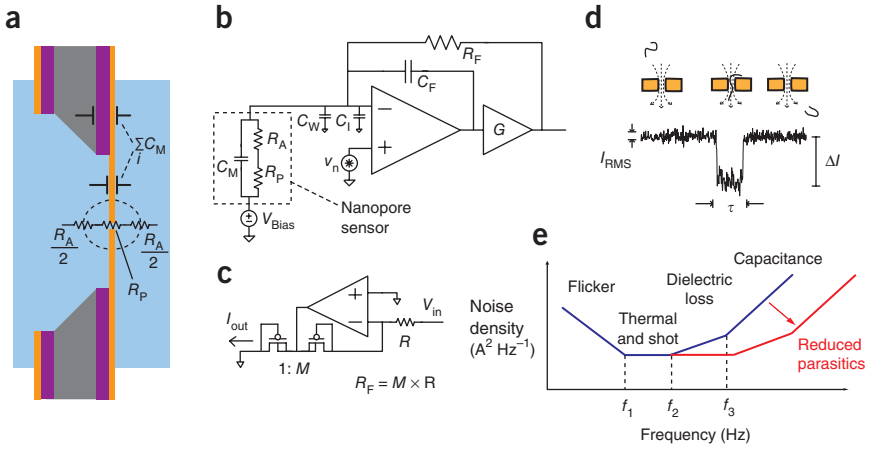

Figure 2 | Electrical modeling of a nanopore measurement. (**a**) An illustration of the electronic impedances of a solid-state nanopore chip. (**b**) Simplified circuit schematic of the voltage-clamp current preamplifier. (**c**) Circuit design of the low-noise current source that substitutes for a feedback resistance (R_F). (**d**) An example transient current pulse, characteristic of a single-molecule event such as the one illustrated. (**e**) Dominant sources of noise power spectral density, illustrated as a function of frequency.

electrode is fabricated on the surface of the amplifier and this wiring distance is less than 100 µm. However, the exposure of the amplifier to the fluid chamber means that the ions in the electrolyte can capacitively couple to the internal wiring of the integrated circuit. To minimize this effect, we covered most of the amplifier surface with a thick layer of epoxy-based photoresist (Online Methods). The resulting C_W was <1 pF.

Amplifier design

A central component of the CNP is a 3 mm × 3 mm custom integrated circuit fabricated in a 0.13 µm CMOS process. It contains eight low-noise preamplifiers that each occupy 0.2 mm^2 and implement a voltage-clamped transimpedance circuit (**Fig. 2b**). For the experiments presented here, we used only one channel; however, the channels are independent and can be operated in parallel. We adapted several elements of a classical transimpedance topology to make the design suitable for modern integrated circuit technology. In particular, the design must function without the availability of a high-value feedback resistor (R_F). Purely capacitive feedback would be appropriate if not for the considerable steady-state bias currents of nanopore sensors. Thus, in place of a traditional feedback resistor, the CNP implements a servo loop with an active low-noise current source[16], producing a closed-loop circuit with a gain of 100 MΩ (**Fig. 2c**). A digitally selectable feedback capacitor C_F and a gain element G prevented oscillation by reducing the closed-loop gain above 30 kHz, and the preamplifier was followed by a filter to restore a flat gain response to >1 MHz (Online Methods). We designed the input stage for negligible gate leakage and an input capacitance of C_I = 1 pF, and commonly operated it with C_F = 0.15 pF. The amplifier had v_n = 5 nV $\sqrt{\text{Hz}}^{-1}$, and it consumed 5 mW from a 1.5 V supply.

Noise measurements

The measured baseline noise spectrum of the CNP system compared favorably with a similar open-headstage configuration of an Axopatch 200B (**Fig. 3a–c**). At measurement bandwidths below 10 kHz, the noise of the Axopatch was lower than that of the CNP, owing to the 100 fA^2 Hz^{-1} white-noise density of the CNP's on-chip current source (**Fig. 2c**) as compared to 33 fA^2 Hz^{-1} from a discrete 500 MΩ feedback resistor in the Axopatch. However, for B > 10 kHz, the CNP delivered much lower noise. For the highest

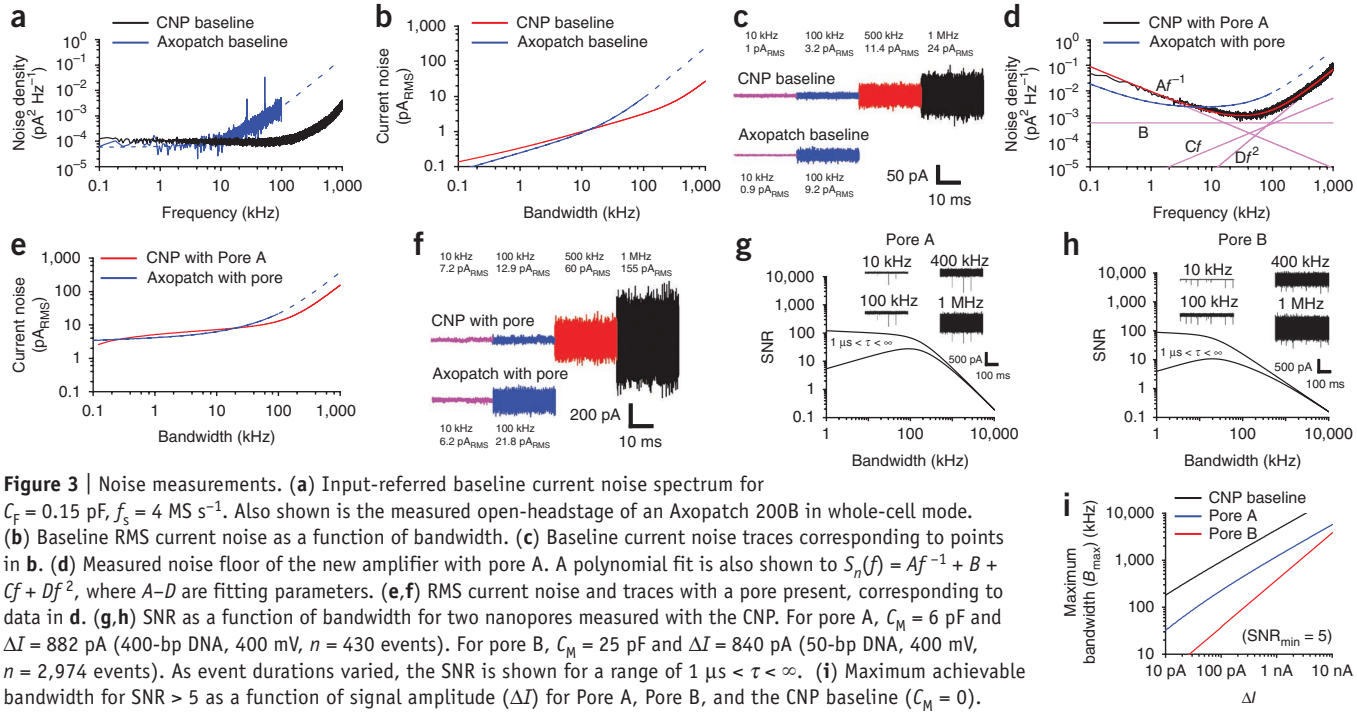

Figure 3 | Noise measurements. (**a**) Input-referred baseline current noise spectrum for C_F = 0.15 pF, f_s = 4 MS s^{-1}. Also shown is the measured open-headstage of an Axopatch 200B in whole-cell mode. (**b**) Baseline RMS current noise as a function of bandwidth. (**c**) Baseline current noise traces corresponding to points in **b**. (**d**) Measured noise floor of the new amplifier with pore A. A polynomial fit is also shown to $S_n(f) = Af^{-1} + B + Cf + Df^2$, where A–D are fitting parameters. (**e**,**f**) RMS current noise and traces with a pore present, corresponding to data in **d**. (**g**,**h**) SNR as a function of bandwidth for two nanopores measured with the CNP. For pore A, C_M = 6 pF and ΔI = 882 pA (400-bp DNA, 400 mV, n = 430 events). For pore B, C_M = 25 pF and ΔI = 840 pA (50-bp DNA, 400 mV, n = 2,974 events). As event durations varied, the SNR is shown for a range of 1 µs < τ < ∞. (**i**) Maximum achievable bandwidth for SNR > 5 as a function of signal amplitude (ΔI) for Pore A, Pore B, and the CNP baseline (C_M = 0).

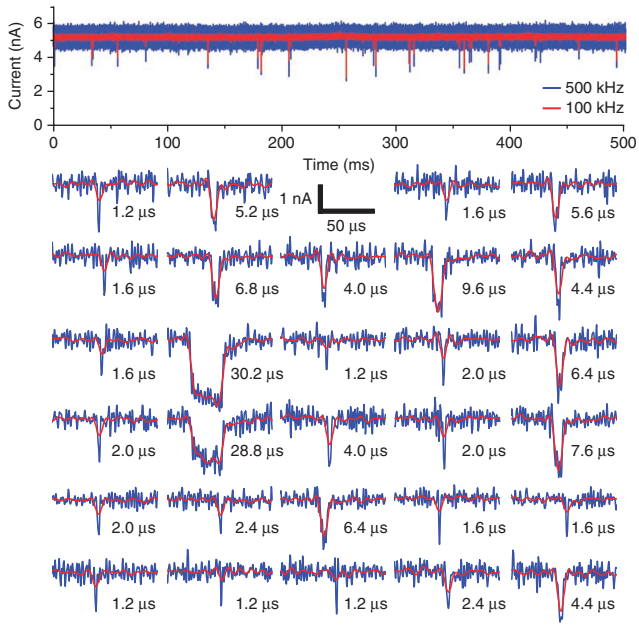

Figure 4 | Fast single-molecule events. A continuous trace recorded with 25-bp dsDNA fragments and pore B using the CNP platform, at a bias of 600 mV. The traces are recorded at 2.5 MS s^{-1} and digitally filtered to both B = 500 kHz and 100 kHz. Insets of the 29 translocation events in this 500-ms trace are displayed.

bandwidth supported by the Axopatch (100 kHz), the CNP had a noise floor of 3.2 pA_{RMS}, compared to 9 pA_{RMS} for the Axopatch. At the highest bandwidth characterized for the CNP (1 MHz), the noise level was 24 pA_{RMS}, in contrast with 247 pA_{RMS} modeled by extrapolating the Axopatch response beyond its supported range (**Supplementary Discussion**).

When we connected a nanopore to the amplifier input, flicker noise and membrane capacitance raised the noise spectrum above the baseline (**Fig. 3d–f**). We measured ~15 solid-state nanopores with the CNP, and observed considerable pore-to-pore SNR variability, owing to variations in the pore geometry and in C_M. For the discussions that follow, we selected data from two representative nanopore devices for analysis. 'Pore A' (4.9 nm diameter, C_M = 6 pF) had lower membrane capacitance than 'pore B' (3.5 nm diameter, C_M = 25 pF).

With the lowest-capacitance nanopores measured, such as pore A, we observed noise of 12.9 pA_{RMS} and 155 pA_{RMS} for bandwidths of 100 kHz and 1 MHz, respectively. For B = 100 kHz, there was more than a factor-of-two reduction in input-referred noise power for the CNP as compared to the Axopatch. If the Axopatch could be measured at higher bandwidths, there would have been a factor-of-six noise power difference at 1 MHz.

Aside from the overall lower noise at high frequencies, we observed that polynomial fits to the noise power spectrum (**Fig. 3d**) did not contain a substantial linear component at moderate frequencies (>1 kHz), which dominated the high-frequency noise in earlier reports[12,14]. This is likely attributable to the high-quality dielectric properties of the thermal SiO_2 passivation of the nanopore support chip (**Supplementary Discussion**).

To determine bandwidths that could be supported, we calculated the SNR for each pore as a function of signal bandwidth (**Fig. 3g,h**). For pore A, SNR was maintained above 10 beyond 600 kHz bandwidth and above 5 beyond 1 MHz. For pore B, SNR values of 10 and 5 were maintained up to 160 kHz and 320 kHz, respectively. In the limit of very small C_M, the baseline amplifier noise floor corresponded to usable measurement bandwidth of several megahertz (**Fig. 3i**).

Short-DNA measurements

As an example of the short timescales observable with the CNP, we considered a current trace measured for pore B with 25 base pair (bp) dsDNA (**Fig. 4**). The pore was biased at 600 mV, digitized at 2.5 MS s^{-1}, and then digitally filtered to both 500 kHz and 100 kHz bandwidths. The 500 kHz trace represents the maximum bandwidth for which SNR > 5 in these conditions (ΔI = 1.3 nA, n = 1,307 events), and we also filtered the data to 100 kHz to compare to the supported bandwidth of other platforms. In a 500-ms period (**Fig. 4**), 29 molecules translocated through the pore, producing pulses ranging in duration from 1.2 µs to 30.2 µs. Sample points were separated by intervals of 0.4 µs, but the rise and fall times were ~1 µs and ~5 µs for the 500-kHz trace and 100-kHz trace, respectively. Accordingly, events shorter than 10 µs were clearly visible in the 500-kHz trace, but their amplitude was attenuated at 100 kHz. Similarly sized oligomers have been previously measured with solid-state nanopores[7,17], but observed pulse durations regularly saturate at the 10–100 µs temporal resolution of the measurements. In some prior instances, experiments have been performed at 0 °C, increasing the viscosity of the electrolyte and slowing the kinetics of surface interactions[18]. In contrast, we collected the data presented here at room temperature (20–23 °C).

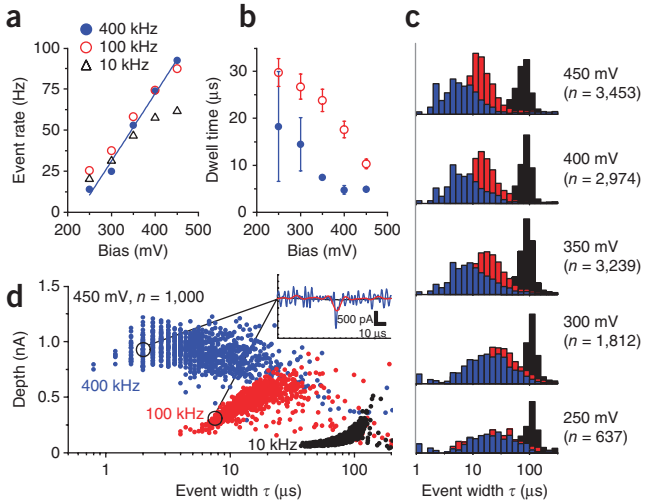

Figure 5 | Fast nanopore event statistics (50 bp dsDNA and pore B). (**a–c**) The CNP output was sampled at 2.5 MS s^{-1} and then digitally filtered to B = 400 kHz, 100 kHz and 10 kHz signal bandwidths. Event rate as a function of applied bias, for a detection threshold of 5σ (**a**). Characteristic dwell time τ_1 at 400 kHz and 100 kHz as a function of applied potential (**b**). τ_1 was calculated from the width distribution $P(\tau) = A \exp(-\tau/\tau_1) + B \exp(-\tau/\tau_2)$, where τ_1 is the shorter time constant[18]. Error bars, s.e.m. of the fitted parameter (n > 500). Histograms of event widths at applied potentials of 250–450 mV (**c**). (The listed event count n is for the 400 kHz data. In the 250–300 mV data the heights of the 10 kHz bins were reduced by half for visual clarity.) (**d**) A scatter plot of events from a subset of the 450 mV data at the three bandwidths. Brief events were severely distorted and attenuated by lower bandwidths. Inset, representative event in the 450 mV dataset. The event was notably distorted at 100 kHz, and undetected at 10 kHz.

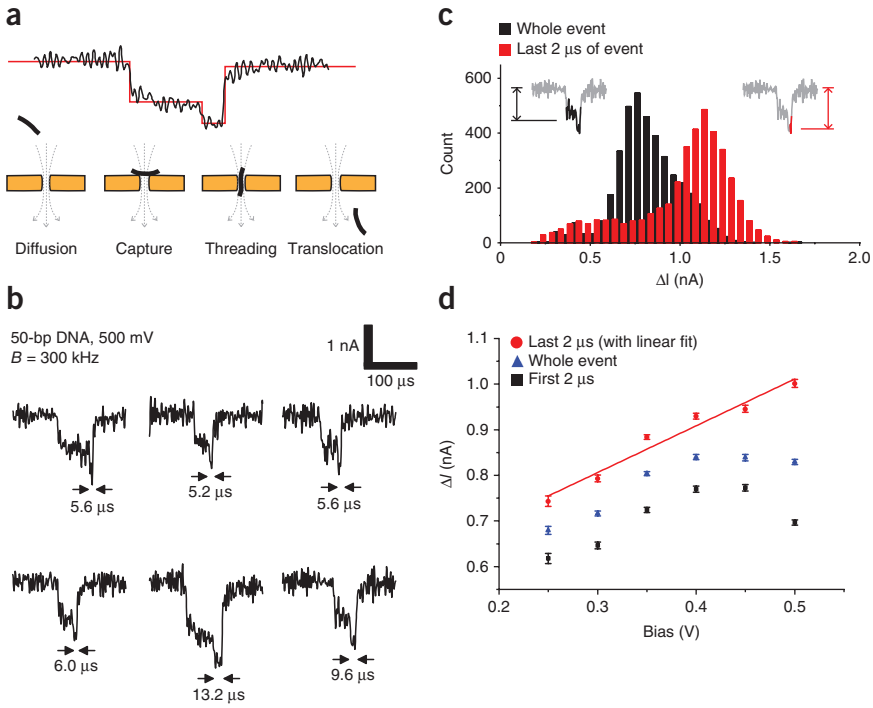

Figure 6 | Intra-event structure. (**a**) An illustration of the sequential processes of translocation for short oligomers and small nanopores. (**b**) Typical signals observed for 50-bp dsDNA fragments with pore B (d = 3.5 nm) at 500 mV bias. (**c**) A histogram of event depths (ΔI) for 50-bp DNA at 500 mV bias (n = 3,955 events). The depth of the whole events and the depth of the last 2 µs of each event have distinct distributions. (**d**) A plot of the mean depths of the whole events, along with the mean depths of the first and last 2 µs of each event (error bars, s.e.m, n > 500). The depth of the last 2 µs retained a linear relationship with voltage up to 500 mV, whereas earlier portions of the events became shallower at high bias. This may be indicative of molecular dynamics at high electric fields which suppress polymer diffusion and extend the duration of the 'capture' phase relative to the 'threading' phase.

DNA translocation statistics

Finer temporal resolution allowed us to consider the statistics of shorter duration events than have been previously characterized. At 3.5 nm diameter, pore B was small enough that oligomer translocation times were dominated by surface interactions rather than electrophoretic forces[18,19]. As such, we observed a wide variance in translocation times (**Fig. 5**). Analyisis of this dataset at several different signal bandwidths resulted in a useful illustration of the impact of measurement bandwidth on observed properties of events.

We observed a linear event rate trend with voltage that indicated a diffusion-limited capture regime above an energy barrier[20] of 200 mV (**Fig. 5a**). Although the observed event rates were similar at 400-kHz and 100-kHz bandwidths, the apparent durations and depths of brief events were quite different. Events as short as 2 µs were clearly distinguished at 400 kHz, whereas at 100-kHz, events faster than 10 µs were strongly attenuated and distorted[21]. This had a marked effect on the observed statistics of the events, exaggerating the duration of short events in the 100-kHz dataset (**Fig. 5b**,**c**). Above 400 mV, we continued to observe events below the 2.5 µs response of the 400-kHz filter (**Fig. 5d**), implying that some of the observed pulses were likely sub-microsecond events that could be better resolved if the membrane capacitance were further decreased.

Intra-event translocation dynamics

Although it is simplest to characterize nanopore current blockades as elementary pulses, it is generally acknowledged that, absent noise and bandwidth limitations, the current would be observed to vary within individual blockades owing to changes in the local structure and position of the captured molecule. Previous experiments have distinguished multiple current levels that correspond to folded polymers[22], duplex dissociation[23], distinct regions in a single polymer[24] or conformations of adjacent protein complexes[6].

Similarly, for small-diameter nanopores, both molecular-dynamics simulations[19] and experiments[18] have observed that even brief translocation events consist of several sequential processes. We extended the dataset from pore B with 50-bp dsDNA (**Fig. 5**) to 500 mV bias (**Fig. 6**). At this high voltage, we commonly observed translocations with an initial shallow blockage followed by a deeper tail immediately before completion. A reasonable explanation for this intra-event structure is a multistate process (**Fig. 6a**). First, a diffusing molecule is captured by the nanopore in a sideways orientation, which does not permit translocation, leading to shallow blockade. Then, after the molecule reorients lengthwise, it fully enters the pore and causes a deeper blockade. We observed this event structure more frequently at higher voltage bias (**Fig. 6b**), which is consistent with a model of an inflexible molecule becoming trapped near the pore opening by high electric fields and frictional forces (duplex DNA has a persistence length of 50 nm, and thus a 15-nm-long 50-bp molecule can be approximated as a rigid rod).

In the dataset derived from 50-bp DNA fragments, the deeper tail was often faster than 10 µs, and it was commonly obscured in low-bandwidth measurements. We analyzed the event tails by computing the mean current of the final 2 µs of each event, and we concluded that the depth of the tail was distinct from the depth of the event as a whole (**Fig. 6c**). The depth of the last 2 µs exhibited a linear relationship with bias voltage, whereas the remainder of the event did not (**Fig. 6d**). This supports the hypothesis that the deeper tail signaled the passage of the molecule through the pore, and that in strong electric fields it became increasingly likely that a molecule would be trapped at the mouth of the pore before translocating through it.

DISCUSSION

With commonly achieved temporal resolution of tens of microseconds, ion channels and nanopores already represent some of the highest bandwidth single-molecule sensing platforms available. By introducing a high-performance CMOS preamplifier directly into the electrochemical environment, we extended nanopore signal bandwidths by at least an order of magnitude. Similar optimizations are directly applicable to measurements of biological ion channels[25], especially channels that may exhibit fast

conductance fluctuations that are poorly resolved at lower bandwidths. Other electrochemical transducers, such as those based on tunneling junctions[26], nanowires[27] or carbon nanotubes[28], rely on similar electronic circuits, and their larger signal currents could potentially bring single-molecule measurements deep into nanosecond temporal resolutions.

There are many basic research opportunities presented by high-bandwidth bioelectronic interfaces, including the ability to study fast reaction kinetics, single-molecule transport phenomena or rapid conformational changes of macromolecules. Extending single-molecule measurements to megahertz bandwidths can bridge the gap to molecular dynamics simulations, which are often limited to nanosecond timescales for computational reasons[29]. Benefits would be seen in single-molecule recapture systems[30] or closed-loop electrostatic traps[31], as the measurement latency in such a system limits its control of fast-diffusing small molecules. Higher bandwidth also allows more precise measurements of the relative timing of events in a multichannel system.

In the context of nanopore DNA sequencing, lower noise spectral density will yield more accurate base calls, and with sufficient signal amplitudes, wider signal bandwidth can support faster translocations and thus higher throughput. As even well-controlled polymer translocation may be somewhat stochastic[6], faster measurements will also decrease the likelihood of deletions in a nanopore sequence output.

From a practical standpoint, an important aspect to the promise of nanopore sensors is the ability to scale to arrays of many devices operating in parallel. If implemented in a fully dense array, the design presented here would yield 500 preamplifiers per square centimeter, and additional optimizations would enable several thousand independent channels per square centimeter. Paired with appropriate fluidics and an array of biological or solid-state nanopores, this would represent an extraordinarily high-throughput single-molecule sensing platform.

METHODS

Methods and any associated references are available in the online version of the paper at http://www.nature.com/naturemethods/.

Note: Supplementary information is available on the Nature Methods website.

ACKNOWLEDGMENTS

We thank K. Venta, M. Puster, K. Healy, V. Ray, C. Dean and L. Paninski for their assistance. K.L.S. acknowledges partial support from the Semiconductor Research Corporation through the Focus Center Research Program, the US National Institutes of Health (R33HG003089) and the Office of Naval Research (N00014-09-1-1117). M.D. acknowledges support from the National Institutes of Health (R21HG004767, American Recovery and Reinvestment Act Supplement to R21HG004767 and R21HG006313).

AUTHOR CONTRIBUTIONS

J.K.R., K.L.S. and M.D. developed the platform concept. J.K.R. designed the amplifier and measurement system. J.K.R., K.L.S., M.W. and M.D. planned experiments. M.W. and C.A.M. fabricated nanopores. J.K.R. and M.W. performed nanopore experiments and analyzed data. J.K.R. and K.L.S. wrote the manuscript. All authors edited the manuscript.

COMPETING FINANCIAL INTERESTS

The authors declare no competing financial interests.

Published online at http://www.nature.com/naturemethods/.
Reprints and permissions information is available online at http://www.nature.com/reprints/index.html.

1. Weiss, S. Fluorescence spectroscopy of single biomolecules. *Science* **283**, 1676–1683 (1999).
2. Kasianowicz, J.J., Brandin, E., Branton, D. & Deamer, D.W. Characterization of individual polynucleotide molecules using a membrane channel. *Proc. Natl. Acad. Sci. USA* **93**, 13770–13773 (1996).
3. Howorka, S. & Siwy, Z. Nanopore analytics: sensing of single molecules. *Chem. Soc. Rev.* **38**, 2360–2384 (2009).
4. Branton, D. *et al.* The potential and challenges of nanopore sequencing. *Nat. Biotechnol.* **26**, 1146–1153 (2008).
5. Venkatesan, B.M. & Bashir, R. Nanopore sensors for nucleic acid analysis. *Nat. Nanotechnol.* **6**, 615–624 (2011).
6. Cherf, G.M. *et al.* Automated forward and reverse ratcheting of DNA in a nanopore at 5-Å precision. *Nat. Biotechnol* advance online publication, doi:10.1038/nbt.2147 (14 February 2012).
7. Wanunu, M. *et al.* Rapid electronic detection of probe-specific microRNAs using thin nanopore sensors. *Nat. Nanotechnol.* **5**, 807–814 (2010).
8. Sakmann, B. & Neher, E. *Single-Channel Recording* (Springer, 2009).
9. Hille, B. *Ion Channels of Excitable Membranes* 3rd edn. (Sinauer, 2001).
10. Derrington, I.M. *et al.* Nanopore DNA sequencing with MspA. *Proc. Natl. Acad. Sci. USA* **107**, 16060–16065 (2010).
11. Kowalczyk, S.W., Grosberg, A.Y., Rabin, Y. & Dekker, C. Modeling the conductance and DNA blockade of solid-state nanopores. *Nanotechnology* **22**, 315101 (2011).
12. Smeets, R., Keyser, U., Dekker, N. & Dekker, C. Noise in solid-state nanopores. *Proc. Natl. Acad. Sci. USA* **105**, 417–421 (2008).
13. Hoogerheide, D., Garaj, S. & Golovchenko, J. Probing surface charge fluctuations with solid-state nanopores. *Phys. Rev. Lett.* **102**, 256804 (2009).
14. Tabard-Cossa, V., Trivedi, D., Wiggin, M., Jetha, N.N. & Marziali, A. Noise analysis and reduction in solid-state nanopores. *Nanotechnology* **18**, 305505 (2007).
15. Dimitrov, V. *et al.* Nanopores in solid-state membranes engineered for single molecule detection. *Nanotechnology* **21**, 065502 (2010).
16. Ferrari, G., Gozzini, F., Molari, A. & Sampietro, M. Transimpedance amplifier for high sensitivity current measurements on nanodevices. *IEEE J. Solid-State Circuits* **44**, 1609–1616 (2009).
17. Heng, J.B. *et al.* Sizing DNA using a nanometer-diameter pore. *Biophys. J.* **87**, 2905–2911 (2004).
18. Wanunu, M., Sutin, J., McNally, B., Chow, A. & Meller, A. DNA translocation governed by interactions with solid-state nanopores. *Biophys. J.* **95**, 4716–4725 (2008).
19. Aksimentiev, A., Heng, J.B., Timp, G. & Schulten, K. Microscopic kinetics of DNA translocation through synthetic nanopores. *Biophys. J.* **87**, 2086–2097 (2004).
20. Heng, J.B. *et al.* Stretching DNA using the electric field in a synthetic nanopore. *Nano Lett.* **5**, 1883–1888 (2005).
21. Pedone, D., Firnkes, M. & Rant, U. Data analysis of translocation events in nanopore experiments. *Anal. Chem.* **81**, 9689–9694 (2009).
22. Li, J., Gershow, M., Stein, D., Brandin, E. & Golovchenko, J.a. DNA molecules and configurations in a solid-state nanopore microscope. *Nat. Mater.* **2**, 611–615 (2003).
23. Vercoutere, W. *et al.* Rapid discrimination among individual DNA hairpin molecules at single-nucleotide resolution using an ion channel. *Nat. Biotechnol.* **19**, 248–252 (2001).
24. Akeson, M., Branton, D., Kasianowicz, J.J., Brandin, E. & Deamer, D.W. Microsecond time-scale discrimination among polycytidylic acid, polyadenylic acid, and polyuridylic acid as homopolymers or as segments within single RNA molecules. *Biophys. J.* **77**, 3227–3233 (1999).
25. Shapovalov, G. & Lester, H.A. Gating transitions in bacterial ion channels measured at 3-microsecond resolution. *J. Gen. Physiol.* **124**, 151–161 (2004).
26. Tsutsui, M., Taniguchi, M., Yokota, K. & Kawai, T. Identifying single nucleotides by tunnelling current. *Nat. Nanotechnol.* **5**, 286–290 (2010).
27. Xie, P., Xiong, Q., Fang, Y., Qing, Q. & Lieber, C.M. Local electrical potential detection of DNA by nanowire–nanopore sensors. *Nat. Nanotechnol.* **7**, 119–125 (2012).
28. Sorgenfrei, S. *et al.* Label-free single-molecule detection of DNA-hybridization kinetics with a carbon nanotube field-effect transistor. *Nat. Nanotechnol.* **6**, 126–132 (2011).
29. Klepeis, J.L., Lindorff-Larsen, K., Dror, R.O. & Shaw, D.E. Long-timescale molecular dynamics simulations of protein structure and function. *Curr. Opin. Struct. Biol.* **19**, 120–127 (2009).
30. Gershow, M. & Golovchenko, J.a. Recapturing and trapping single molecules with a solid-state nanopore. *Nat. Nanotechnol.* **2**, 775–779 (2007).
31. Luan, B. *et al.* Base-by-base ratcheting of single stranded DNA through a solid-state nanopore. *Phys. Rev. Lett.* **104**, 238103 (2010).

ONLINE METHODS

Integrated circuit design. The amplifier was a custom integrated circuit implemented using a commercial IBM 0.13-µm bulk CMOS mixed-signal process. The chip was designed and simulated using the Cadence Virtuoso software package.

Packaging. The amplifier die was wirebonded to a 272-pin ball-grid array (BGA) package. Dam-and-fill doughnut epoxy encapsulation (Hysol FP4451 dam and FP4650 fill) covered the exposed gold wirebonds, leaving the die surface exposed.

By default, the amplifier chip surface had ~6-µm-thick passivation above the top metal interconnect layer. To reduce capacitive coupling to the electrolyte, after doughnut encapsulation the chip surface was passivated with the epoxy-based photoresist SU-8. Under yellow light, a drop of SU-8 2015 (Microchem) was manually applied to the surface of the amplifier die, filling the 300 µm-deep cavity formed by the epoxy dam. A light vacuum was applied in a dessicator for 15 min, followed by an overnight prebake in an oven at 80 °C. The chip was exposed in an MJB-3 UV contact aligner using a chrome-on-glass mask, 2,000 mW cm^{-2} dose, and 360 nm long-pass UV filter (Omega Optical). A post-exposure-bake for 30 min at 50 °C and development in SU-8 Developer (Microchem) yielded a layer of SU-8 ~200–300 µm thick with 300 µm × 300 µm square openings surrounding the 100 µm × 100 µm electrodes.

A watertight fluid chamber was constructed by fastening a 1 cm segment from a polypropylene tube to the top of the BGA package using polydimethylsiloxane (PDMS; Sylgard 184, Dow Corning).

Electrode modifications. After packaging the die, the aluminum was etched from the exposed surface electrodes by pipetting 500 µl of aluminum etchant (type A, Transene) into the fluid chamber for several minutes, followed by multiple rinses with deionized water.

The chip was mounted on a circuit board, powered on, and digital logic was applied to short-circuit the amplifier feedback element C_F, clamping multiple channels' electrodes at a constant voltage and providing a path for them to sink several microamperes of current. A small volume (~1 ml) of silver electroplating solution containing potassium silver cyanide (Transene), was added to the fluid chamber, and a silver wire counterelectrode was attached to a Keithley 2400 I-V meter and placed in the solution. The voltage was adjusted to achieve a counterelectrode current of 1 µA for several minutes, resulting in a deposition of ~10 µm of silver onto each electrode. After electroplating, the chamber was rinsed multiple times with deionized water.

The silver microelectrodes were converted to Ag/AgCl pseudo-reference electrodes by applying a drop of 10 µl 50 mM $FeCl_3$ to the surface for 30 s (ref. 32). After several hours of experiments, the chlorination typically needed to be repeated. We found that the chlorination could be repeated several times before the silver electrode was exhausted.

Images of an electrode at several steps during this process are available in the **Supplementary Discussion**.

Nanopore fabrication. Nanopores in ultrathin silicon nitride membranes were fabricated in a similar manner as described elsewhere[7]. Briefly, a 500-µm-thick silicon wafer with <100> crystal orientation (in which the <> notation refers to a material's three-dimensional crystal orientation) and 5 µm of thermal oxide was coated with 25 nm of low-stress chemical vapor deposition silicon nitride (SiN). Standard UV photolithography was used to pattern square openings on one side of the wafer, through which the nitride and oxide were etched using SF_6 plasma. The photoresist was stripped, and an anisotropic KOH etch followed by removal of the oxide layer resulted in ~50 µm × 50 µm free-standing windows on the reverse side of the wafer.

A film of poly-(methyl methacrylate) (PMMA, Microchem) was spun onto the membrane side of the window, and electron-beam lithography was used to pattern a small square opening of 500 nm × 500 nm or smaller. A SF_6 plasma etch locally thinned the SiN in this region to ~10–15 nm. The confined area of this ultrathin region helped to limit the capacitance of the membrane and maintain its mechanical integrity. The PMMA was removed by incubation in acetone. A single nanopore was drilled through the thinned region of the nitride membrane using a JEOL 2010F HR-TEM. Fabricated pores were 2–6 nm in diameter, but the best signals from duplex DNA were obtained for 3.5–4 nm pores.

Nanopore experiments. The nanopore chip was cleaned in piranha acid using a procedure described previously[33]. After rinsing and drying the membrane, it was immediately mounted onto a custom Teflon fluid cell using KWIK-CAST silicone elastomer (World Precision Instruments). The silicone was carefully painted over the majority of the membrane-facing side of the chip, leaving an exposed <1 mm^2 area around the membrane (**Fig. 1e**). Additionally, for these experiments, silicone was applied on the amplifier chip surface, leaving only one preamplifier channel exposed.

When testing with the Axopatch 200B, the Teflon cell was placed into a mating fluid cell containing 1 M KCl 10 mM Tris buffer, pH 8.0. Inside a Faraday cage, two homemade Ag/AgCl pellet electrodes were connected to the headstage input and ground, respectively.

For testing with the CNP amplifier, the circuit board was placed in a small grounded aluminum box and the lower (*trans*) reservoir was filled with 500 µl 1M KCl, pH 8.0. The upper (*cis*) chamber in the Teflon cell was filled with 200 µl electrolyte, and the cell was placed into the amplifier chamber. An Ag/AgCl pellet electrode was placed in the *cis* chamber. The amplifier input voltage was held constant, as the potential of the opposing electrode was varied to apply a bias across the nanopore.

Supporting electronics and user interface. The preamplifier with its attached fluid chamber was mounted in a compression-mount BGA socket (Emulation Technologies) on a 15 cm × 13 cm circuit board and placed in a small aluminum box. The circuit board contained power regulation, biasing circuitry, analog signal buffering and filters, all of which were carefully designed for low-noise operation. The digital inputs to this board were galvanically isolated, and its outputs were fully differential. The board was powered from four AAA batteries and drew 30 mA. A second interface board outside the aluminum box hosted digital isolators, antialiasing filters (4-pole differential Bessel filter, f_c = 1 MHz) and data converters (operating between 2–4 MS s^{-1}), as well as an FPGA module (Opal Kelly XEM3010) with a 32 MB hardware

data buffer and a high-speed USB interface. The data acquisition and control of the system were managed in real time through a custom graphical interface written in Matlab (MathWorks).

Data processing. The data were processed using custom Matlab software. Traces were generally digitally filtered with a 128- or 512-tap finite-impulse-response low-pass filter to a desired signal bandwidth while retaining the 2–4 MS s^{-1} sample rate. Events were typically identified with a two-state thresholding algorithm in Matlab, but for traces with low SNR, a modified algorithm was used to identify the events: First, samples were identified whose values were more than 5 s.d. below the mean open pore current. Next, a local search found the nearest sample points at which the signal was above the open pore current. Finally, event edge times were assigned at the first and last points in these bounds that the signal was more than 4 s.d. from the baseline current.

32. Polk, B.J., Stelzenmuller, A., Mijares, G., MacCrehan, W. & Gaitan, M. Ag/AgCl microelectrodes with improved stability for microfluidics. *Sensors Actuators Biol. Chem.* **114**, 239–247 (2006).
33. Wanunu, M. & Meller, A. Chemically modified solid-state nanopores. *Nano Lett.* **7**, 1580–1585 (2007).

doi:10.1038/nmeth.1932